

## Supporting Information

### Multimodal Underwater Adsorption of Oxide Nanoparticles on Catechol-Based Polymer Nanosheets

*Shunsuke Yamamoto, Shun Uchiyama, Tokuji Miyashita, Masaya Mitsuishi*

Institute of Multidisciplinary Research for Advanced Materials (IMRAM), Tohoku University,  
2-1-1 Katahira, Aoba-ku, Sendai 980-8577, Japan

#### Details of Polymer Synthesis

Copolymers, p(DDA/DMA<sub>n</sub>)s were obtained by free radical polymerization in anhydrous *N,N*-dimethylformamide (DMF) using azobisisobutyronitrile (AIBN) as initiator. Monomers and AIBN were purified, respectively, by recrystallization from a chloroform/hexane mixture and methanol. The solution of DDA, DMA, and AIBN in DMF was degassed using freeze–pump–thaw cycles five times before the polymerization reaction at 60 °C for 12 h. The total monomer and AIBN concentrations of the solution were set, respectively, to 0.2 M and 2 mM. The resulting solution was concentrated and poured into diethylether (Kanto Chemical Co. Inc.) for reprecipitation. The obtained polymer was reprecipitated two more times. It was then allowed to dry in vacuum overnight. p(DDA/DMA) was obtained as light brown powder. The molecular weight of this polymer was estimated by SEC measurement using a polystyrene standard.

<sup>1</sup>H NMR (400.1 MHz, CDCl<sub>3</sub>) δ 0.88 (t, *J* = 5.6 Hz), 1.25 (s), 1.46 (br), 2.17 (br), 2.71 (br), 3.15 (br), 6.58 (br), and 6.84 ppm (br).

## DLS Data of Nanoparticles

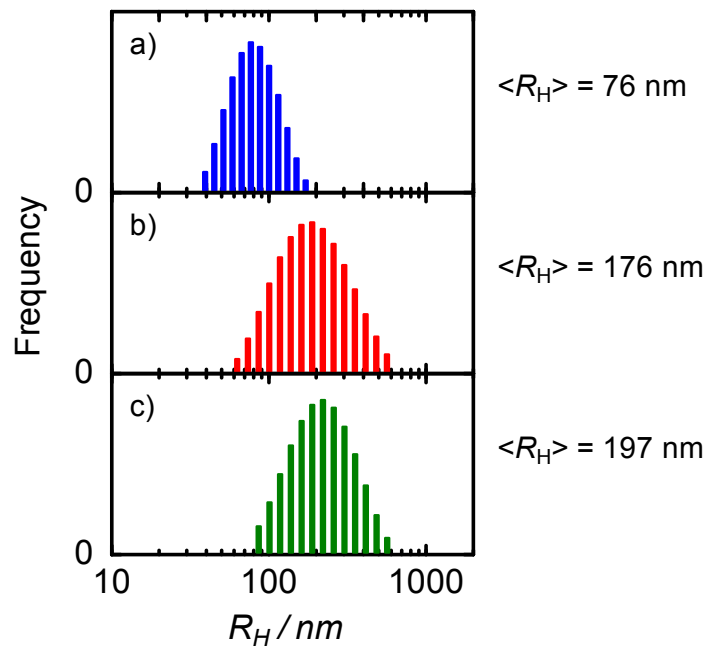


**Figure S1.** Particle size distributions of (a)  $\text{SiO}_2$ , (b)  $\text{Al}_2\text{O}_3$ , and (c)  $\text{WO}_3$  aqueous dispersions measured using DLS.

## FT-IR Spectra

Figure S2 shows the FT-IR spectra of pDDA and p(DDA/DMA32) spincoat films. These two spectra differ slightly at around  $1600\text{ cm}^{-1}$ . This absorption shoulder is observed only for the p(DDA/DMA32) film. To assign this peak, the quantum chemical calculation based on the density functional theory (DFT) was used at the level of B3LYP/6-31+G(d).<sup>S1</sup> As a result, this peak is assigned to the vibration of phenyl rings in DMA.

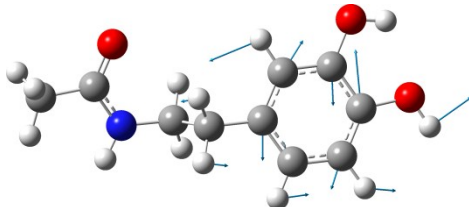
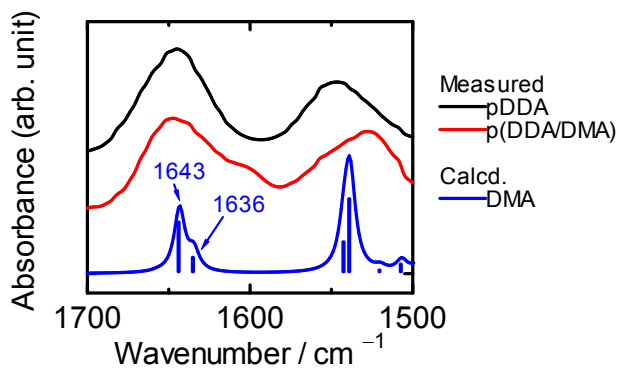


**Figure S2.** (Top) FT-IR spectra of pDDA (black) and p(DDA/DMA32) (red) spincoat films on  $\text{CaF}_2$  plates. The blue line shows simulated IR spectra of DMA monomer by quantum chemical calculation. The wavenumber of blue spectrum is shifted by  $15\text{ cm}^{-1}$  to fit the measured spectra. (Right) Displacement vector of the vibration corresponding to absorption at the  $1636\text{ cm}^{-1}$  peak.

Figure S3 shows IR spectra of p(DDA/DMA32) nanosheets in the transmit and reflection (RAS) modes. The absorption of CH vibration at the  $2800\text{--}3000\text{ cm}^{-1}$  region disappears in the

RAS spectrum, indicating that alkyl side chains are aligned vertically from the substrate surface. This alignment shows good agreement with the results of pDDA nanosheets. The signal attributable to the phenyl ring in DMA unit (shoulder at around  $1600\text{ cm}^{-1}$ ) disappears in the RAS spectrum, which suggests that phenyl rings in DMA units are not aligned vertically from the substrate surface but are instead laid down on the substrate surface plane.

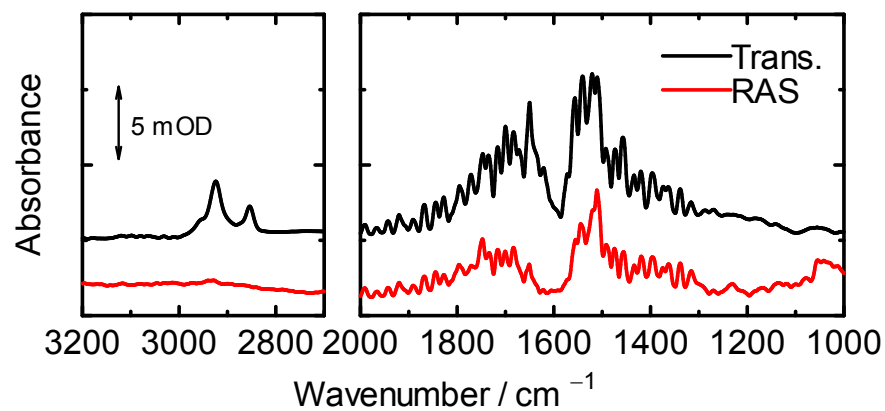


**Figure S3.** FT-IR spectra of 10-layer p(DDA/DMA32) nanosheets in transmission (black) and reflection (red) modes. Nanosheets were fabricated on a  $\text{CaF}_2$  plate (transmission mode) and a glass slide with Cr/Au layers (reflection mode).

## Transfer Curve and UV-vis spectra of p(DDA/DMA) LB Films

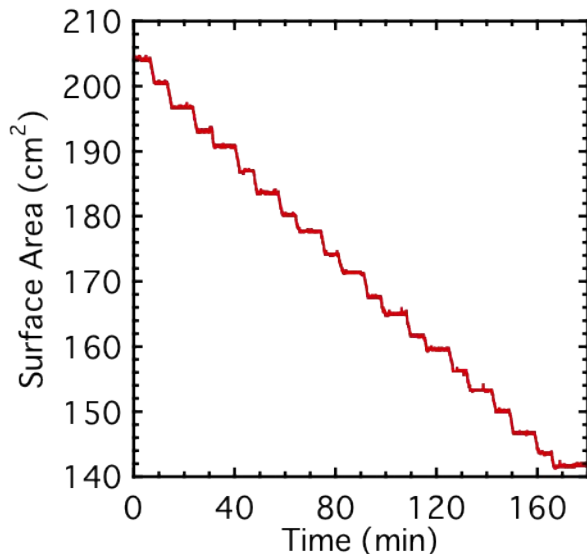


**Figure S4.** Temporal change of p(DDA/DMA32) monolayer on the transferring on Si wafer with hydrophobic surface by silane coupling treatment. The monolayers were transferred at the transfer ratio of approximately 1 up to 20 layers.

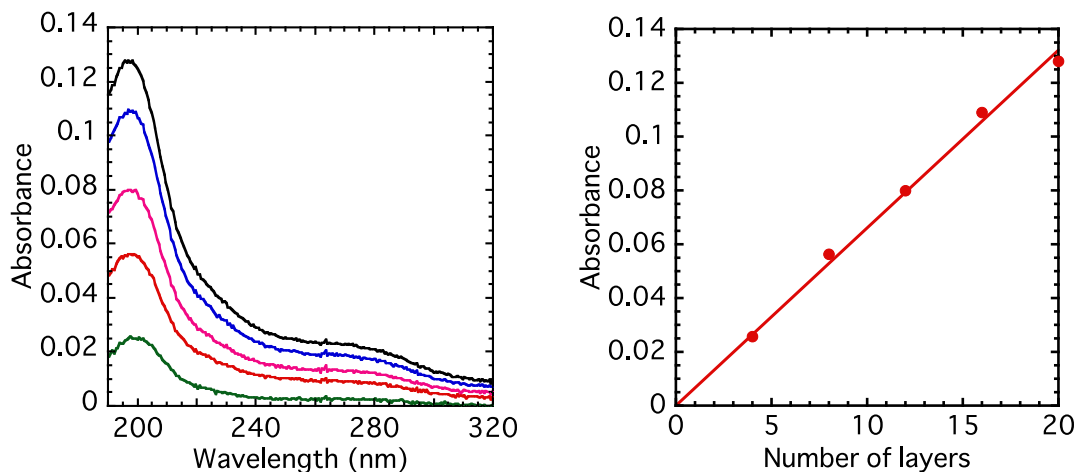


**Figure S5.** (Left) UV-vis absorption spectra of p(DDA/DMA19) nanosheets with 4, 8, 12, 16, and 20 layers. (Right) Plot of absorbance at 192 nm as a function of the number of layers.

### AFM Image of p(DDA/DMA32) Nanosheets

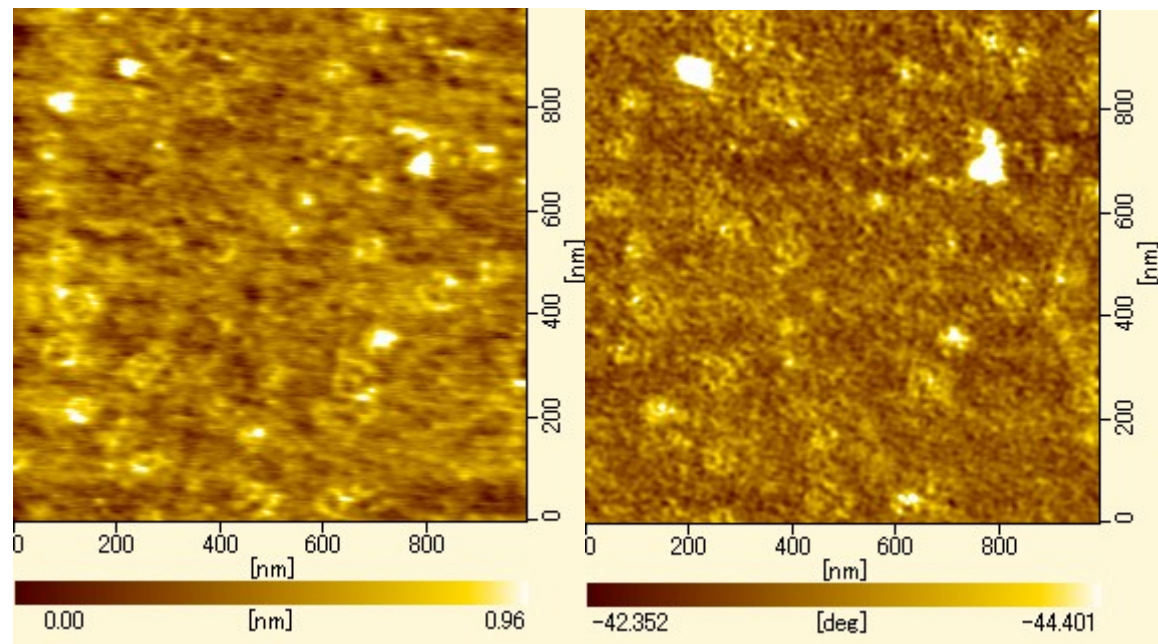


**Figure S6.** (left) Surface topography and (right) phase image of two-layer p(DDA/DMA32) nanosheets deposited on a Si wafer.

## Comparison of Combination Tone of $\text{H}_2\text{O}$ Molecule in pDDA and p(DDA/DMA32) LB Films

Figure S7 depicts FT-IR spectra of pDDA and p(DDA/DMA32) nanosheets. The signals at around 2800 and 3300  $\text{cm}^{-1}$  are assigned, respectively, to vibration of C–H bond and amide groups. The p(DDA/DMA32) nanosheets have a broad peak at around 5000  $\text{cm}^{-1}$ , although no marked peak is observed for pDDA nanosheets.

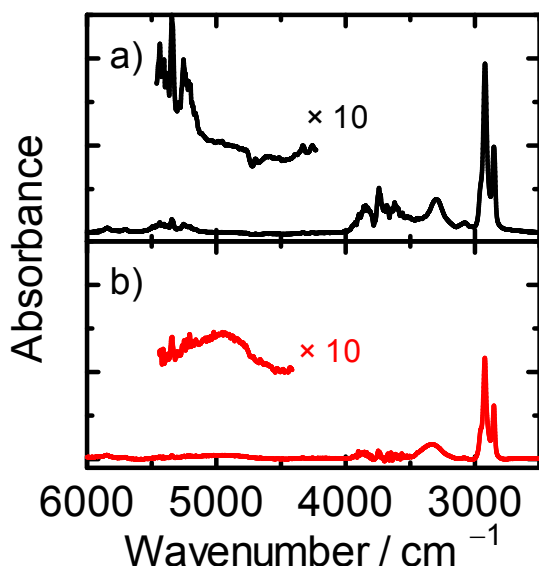


**Figure S7.** FT-IR spectra of 20-layer (a) pDDA and (b) p(DDA/DMA32) nanosheets on  $\text{CaF}_2$  substrates.

## Fitting Parameters for Figure 4

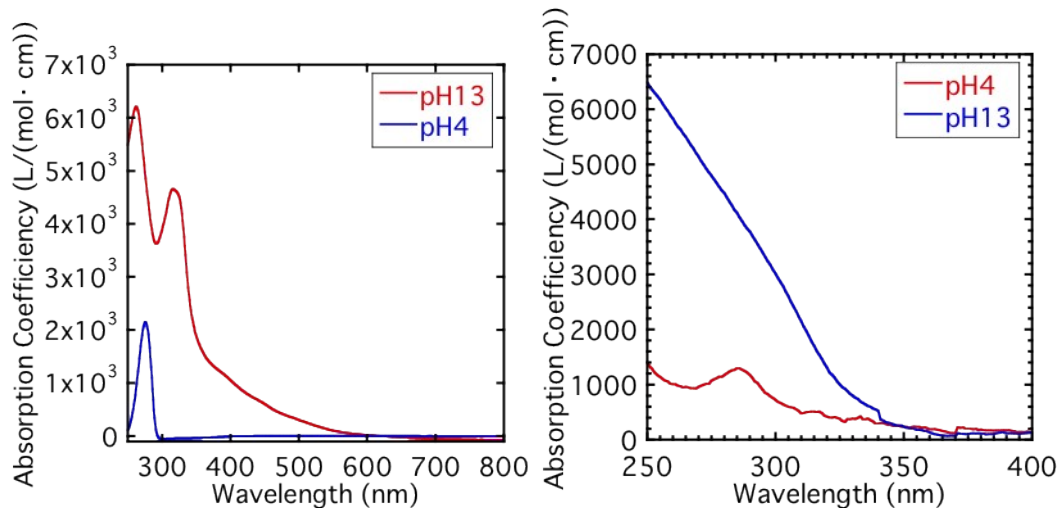
**Table S1.** Fitting parameters by Gaussian functions for Figure 4

peak	Intensity (arb. unit)	Peak Position / cm <sup>-1</sup>	FWHM / cm <sup>-1</sup>	Number of Co-ordination <sup>a</sup>
S <sub>2</sub>	1	4920	276	3–4
S <sub>1</sub>	0.31	5100	202	1
S <sub>0</sub>	0.36	5230	243	0

<sup>a</sup> Based on references 39–42.

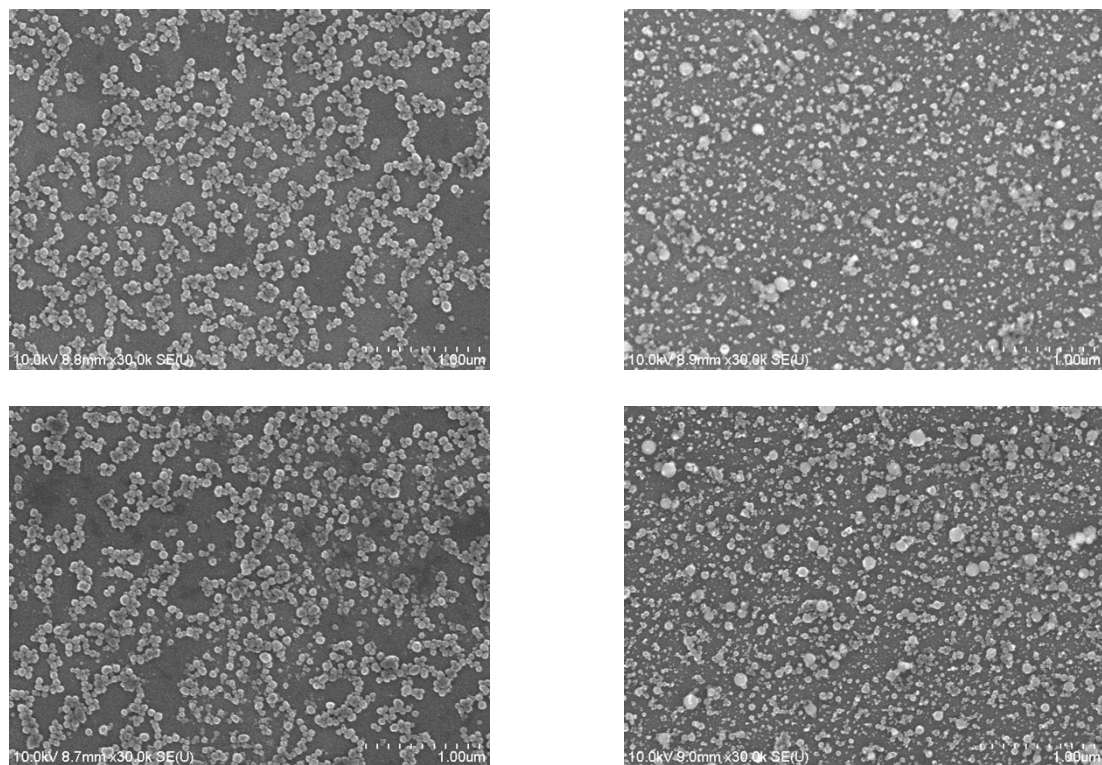
## UV-vis Spectra of p(DDA/DMA32) Nanosheets in Acidic and Basic Conditions

Figure S8 shows UV-vis spectra of catechol in solution and p(DDA/DMA32) nanosheets. in an acidic condition, absorption appears only at around 280 nm, which is assigned to absorption of the catechol form. However, in a basic condition, new absorption appears at around 320 nm, which is assigned to the absorption of the quinone form.



**Figure S8.** UV-vis spectra of catechol solution (left) and p(DDA/DMA32) nanosheets (right) in acidic and basic conditions.

### SEM Image of Sample after Additional Rinse Process



**Figure S9.** SEM image of p(DDA/DMA32) nanosheets after immersion in  $\text{SiO}_2$  (left) and  $\text{Al}_2\text{O}_3$  (right) dispersion at pH = 6.4 after regular procedure (upper) and after additional rinsing and drying processing (lower).

### SEM Image of Sample after Long Immersion

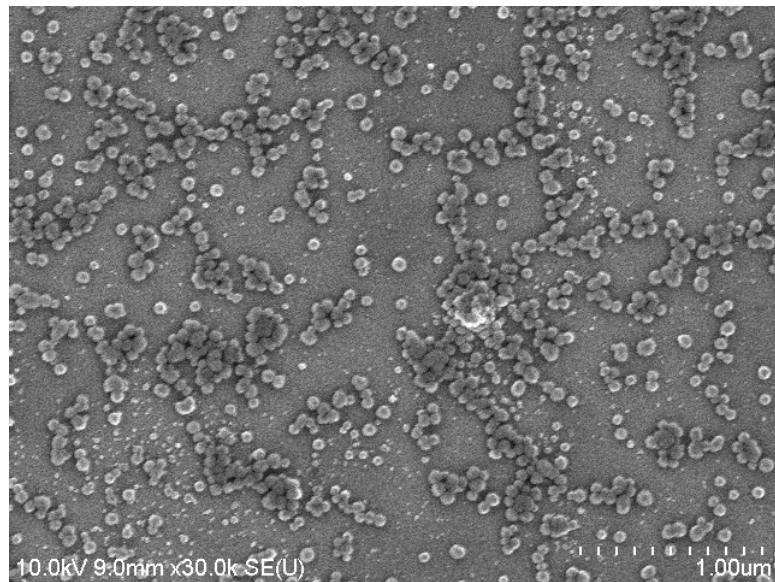


**Figure S10.** SEM image of p(DDA/DMA32) nanosheets after immersion in  $\text{SiO}_2$  dispersion for 3 min.

### Contact Angle of Polymer Nanosheets with SiO<sub>2</sub> Nanoparticles

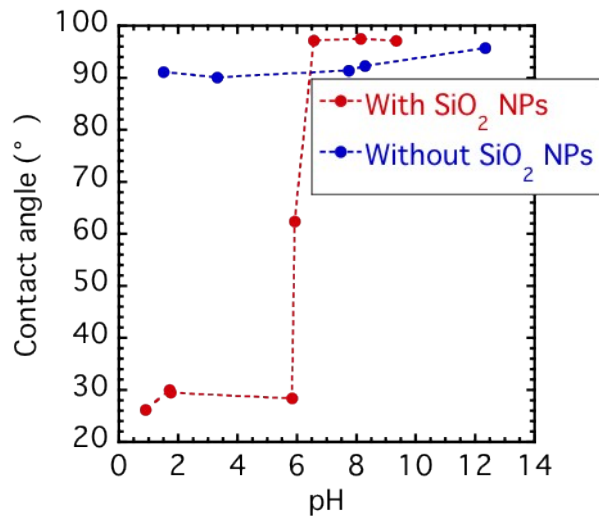


**Figure S11.** Water contact angle of two-layer p(DDA/DMA9) nanosheets after immersion in water (blue) and SiO<sub>2</sub> dispersion (red).

### Layer Number Dependence of SiO<sub>2</sub> NPs Adsorption on p(DDA/DMA9) Nanosheets

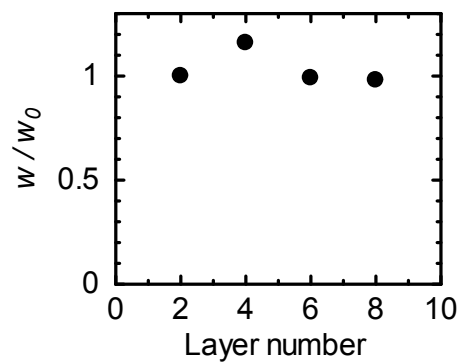


**Figure S12.** Normalized adsorbed amount of SiO<sub>2</sub> NPs on p(DDA/DMA9) nanosheets with different numbers of layers.

### Surface Potential of pDDA Nanosheets

Figure S10 shows the surface potential of pDDA nanosheets on hydrophobic glass substrates with octyltrichlorosilane. For this measurement, samples were immersed in the aqueous dispersion of monitor particle with  $10^{-2}$  M of NaCl. In the thick region ( $>20$  layers), the surface potential was kept constant at -10 mV, which indicates that the surface of pDDA nanosheets charged negatively even if the substrate effect is negligible. For more detailed discussion, the experimental data were fitted by the following equation.

$$\zeta = \zeta_0 \exp(-t/r_D) + \zeta_{pDDA} \quad (S1)$$

Therein,  $\zeta_{pDDA}$  is the surface potential of pDDA nanosheets;  $r_D$  is the Debye length, which is estimated as  $r_D = 2.14$  layers (3.69 nm). That length is comparable to the Debye length in aqueous solution of  $10^{-2}$  M of NaCl (3.04 nm)<sup>S2</sup>, suggesting that the charge on glass substrates can be screened out with an approximately 10-layer pDDA nanosheets in solution.

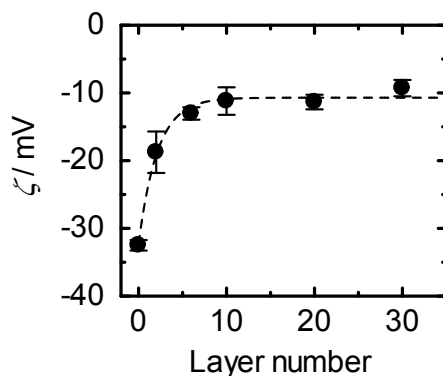


**Figure S13.** Surface potential of pDDA nanosheets on glass substrates with octyltrichlorosilane treatments. The broken line shows fitting by Equation S1.

### SEM Images of $\text{Al}_2\text{O}_3$ Nanoparticles on Polymer Nanosheets

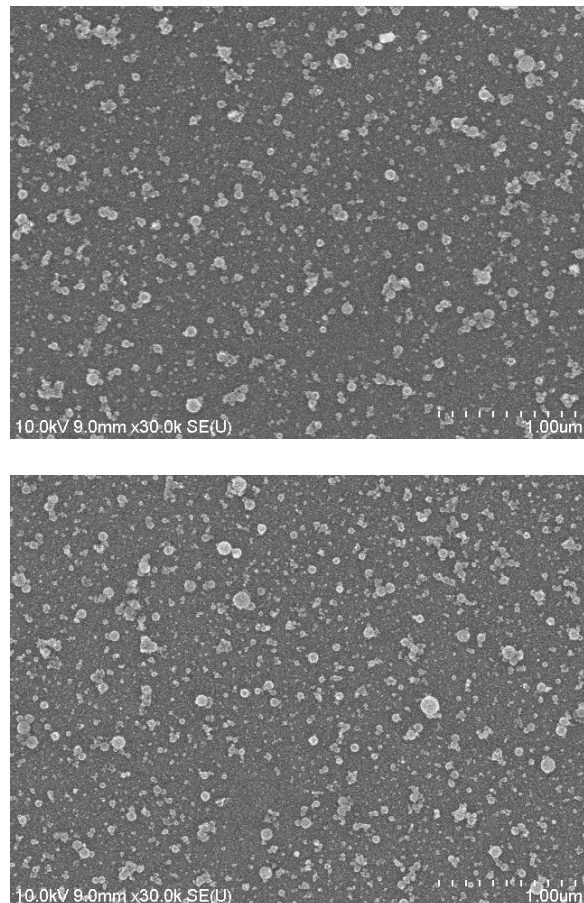


**Figure S14.** SEM images of  $\text{Al}_2\text{O}_3$  nanoparticles assembled on (upper) pDDA and (lower) p(DDA/DMA32) nanosheets at pH = 4.3.

### Surface Coverage of $\text{Al}_2\text{O}_3$ NPs on pDDA Nanosheets

Figure S12 presents the surface coverage of  $\text{Al}_2\text{O}_3$  nanoparticles on pDDA nanosheets estimated from SEM observations. For this measurement, samples were immersed in the aqueous dispersion of  $\text{Al}_2\text{O}_3$  NPs at  $\text{pH} = 4$ . The coverage decreased to 2% for 60-layer pDDA nanosheets. To distinguish the effects of the substrate and pDDA nanosheets, the surface coverage  $c$  is fitted by the following equation.

$$c = c_0 \exp(-t/r_D) + c_{pDDA} \quad (\text{S2})$$

In that equation,  $c_{pDDA}$  denotes the surface coverage on pDDA nanosheets without the substrate effect;  $r_D$  is the Debye length. The value of  $r_D$  is estimated as  $r_D = 16.5$  layers (28.4 nm), which is comparable to the Debye length in aqueous solution of  $10^{-4}$  M of HCl (30.4 nm)<sup>S2</sup>.

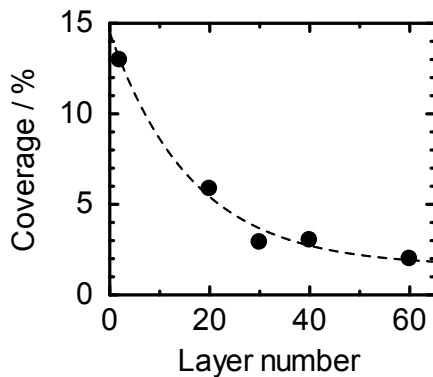


**Figure S15.** Surface coverage of  $\text{Al}_2\text{O}_3$  NPs on pDDA nanosheets. The broken line shows fitting by Equation S2.

**SEM Images of  $\text{Al}_2\text{O}_3$  Nanoparticles on Polymer Nanosheets at High Salt Concentrations**

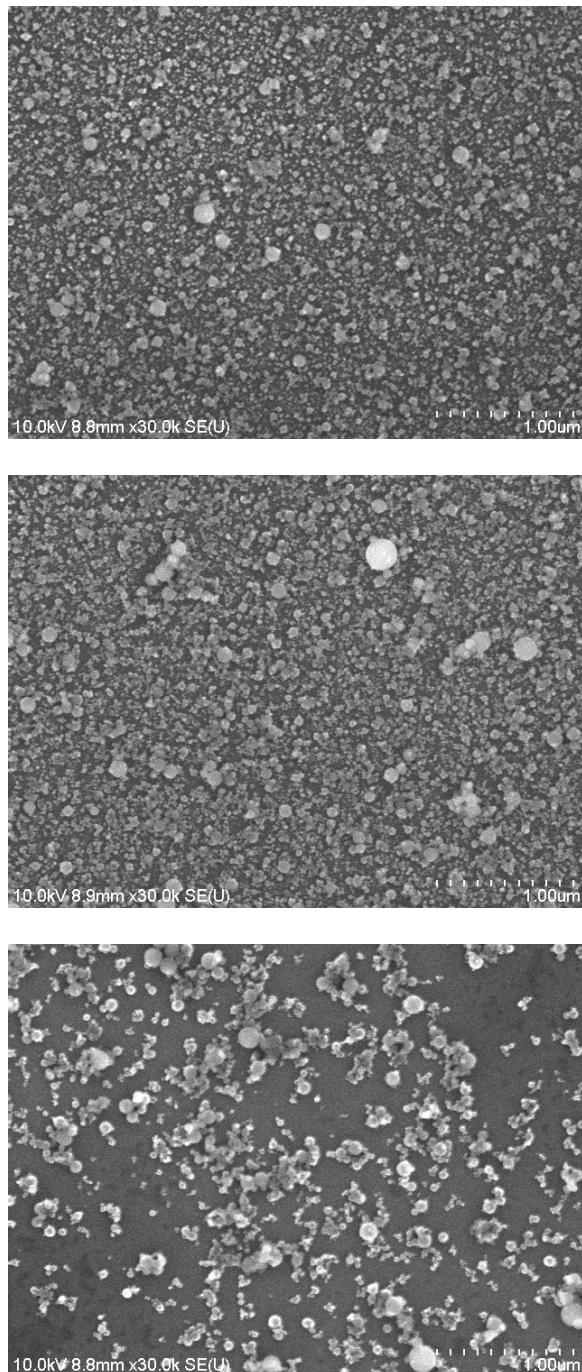


**Figure S16.** SEM images of  $\text{Al}_2\text{O}_3$  nanoparticles assembled on p(DDA/DMA32) nanosheets at pH = 6.4. KCl was added to the dispersion of  $\text{Al}_2\text{O}_3$  nanoparticles as salt at a concentration of (upper) 5, (middle) 10, and (lower) 50 mM.

### SEM Images of $\text{WO}_3$ Nanoparticles on Polymer Nanosheets

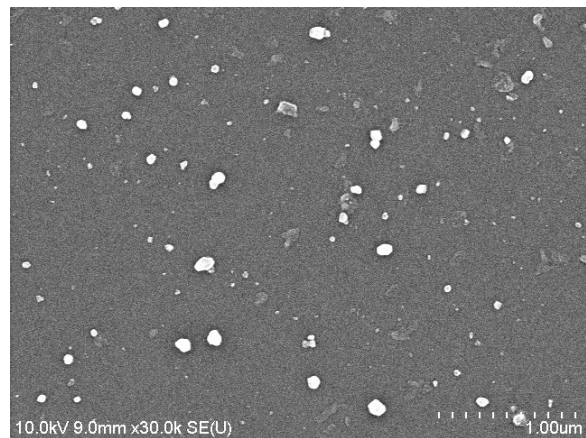


**Figure S17.** SEM images of  $\text{WO}_3$  nanoparticles assembled on p(DDA/DMA32) nanosheets at pH = 3.4, controlled by citric acid.

## References

[S1] Gaussian 09, Revision D.01, M. J. Frisch, G. W. Trucks, H. B. Schlegel, G. E. Scuseria, M. A. Robb, J. R. Cheeseman, G. Scalmani, V. Barone, B. Mennucci, G. A. Petersson, H. Nakatsuji, M. Caricato, X. Li, H. P. Hratchian, A. F. Izmaylov, J. Bloino, G. Zheng, J. L. Sonnenberg, M. Hada, M. Ehara, K. Toyota, R. Fukuda, J. Hasegawa, M. Ishida, T. Nakajima, Y. Honda, O. Kitao, H. Nakai, T. Vreven, J. A., Jr. Montgomery, J. E. Peralta, F. Ogliaro, M. Bearpark, J. J. Heyd, E. Brothers, K. N. Kudin, V. N. Staroverov, R. Kobayashi, J. Normand, K. Raghavachari, A. Rendell, J. C. Burant, S. S. Iyengar, J. Tomasi, M. Cossi, N. Rega, N. J. Millam, M. Klene, J. E. Knox, J. B. Cross, V. Bakken, C. Adamo, J. Jaramillo, R. Gomperts, R. E. Stratmann, O. Yazyev, A. J. Austin, R. Cammi, C. Pomelli, J. W. Ochterski, R. L. Martin, K. Morokuma, V. G. Zakrzewski, G. A. Voth, P. Salvador, J. J. Dannenberg, S. Dapprich, A. D. Daniels, Ö. Farkas, J. B. Foresman, J. V. Ortiz, J. Cioslowski, D. J. Fox, Gaussian, Inc., Wallingford CT, 2009.

[S2] J. N. Israelachvili, *Intermolecular and Surface Forces*, Second ed. Academic Press 1992.